

***Xcat*, a novel mouse model for Nance–Horan syndrome inhibits expression of the cytoplasmic-targeted *Nhs1* isoform**

Kristen M. Huang¹, Junhua Wu¹, Melinda K. Duncan², Chris Moy¹, Amalia Dutra³, Jack Favor⁴, Tong Da¹ and Dwight Stambolian^{1,*}

¹F.M. Kirby Center for Molecular Ophthalmology, Scheie Eye Institute, University of Pennsylvania School of Medicine, Philadelphia, PA, USA, ²Department of Biological Sciences, University of Delaware, Newark, DE, USA, ³NHGRI, NIH, Bethesda, MD, USA and ⁴Institute of Human Genetics, GSF-National Research Center for Environment and Health, Neuherberg, Germany

Received October 4, 2005; Revised and Accepted December 4, 2005

Nance–Horan syndrome (NHS) is an X-linked disorder characterized by congenital cataracts, dental anomalies, dysmorphic features and mental retardation. A recent report suggests that the novel gene *NHS1* is involved in this disorder due to the presence of point mutations in NHS patients. A possible mouse model for NHS, *Xcat*, was mapped to a 2.11 Mb interval on the X-chromosome. Sequence and FISH analysis of the X-chromosome region containing the *Xcat* mutation reveal a large insertion between exons 1 and 2 of the mouse *Nhs1* gene. The insertion inhibits the expression of the *Nhs1* isoform containing exon 1 and results in exclusive expression of the alternative isoform containing exon 1A. Quantitative RT–PCR of *Xcat* cDNA shows reduced levels of *Nhs1* transcripts. The *Nhs1* protein is strongly expressed within the cytoplasm of elongating lens fiber cells from wild-type neonate lens, but is significantly reduced within the *Xcat* lens. Transient transfection studies of CHO cells with *Nhs1*–GFP fusion proteins were done to determine whether the amino acids encoded by exon 1 were critical for protein localization. We found the presence of *Nhs1* exon 1 critical for localization of the fusion protein to the cytoplasm, whereas fusion proteins lacking *Nhs1* exon 1 are predominantly nuclear. These results indicate that the first exon of *Nhs1* contains crucial information required for the proper expression and localization of *Nhs1* protein. Inhibition of expression of the exon 1 containing isoform results in the abnormal phenotype of *Xcat*.

INTRODUCTION

Nance-Horan syndrome (NHS; MIM302350) is a rare X-linked disease characterized by congenital cataracts, microphthalmia, microcornea, dental anomalies and shortened fourth metacarpals in hemizygous males (1). The phenotype in heterozygous females is variable because of X-inactivation (2).

The mouse *Xcat* mutation was identified in a dominant cataract mutation screen (3). There is suggestive phenotypic and genetic evidence that the mouse *Xcat* mutant is a model for human NHS. Similar to NHS, *Xcat* mice display total lens opacity in hemizygous males and homozygous females, whereas female carriers manifest phenotypes varying from

barely noticeable opacities to totally opaque lenses, consistent with X-inactivation (4). Cataracts are congenital in NHS, whereas in *Xcat*, structural abnormalities of the primary lens fibers are detected as early as embryonic day 14 (5). Utilizing an interspecific backcross, the *Xcat* locus has been mapped to a 2.11 Mb region syntenic with the NHS critical region (6). Previous attempts to identify the *Xcat* gene have not been successful (7,8).

The human *NHS1* gene, located within the NHS critical region, has recently been identified as the causative gene in the NHS (9–11). In humans, there are two reported *NHS1* isoforms predicting proteins with 1630 (isoform A) and 1335 (isoform B) amino acids. Although the *NHS1* transcript has

*To whom correspondence should be addressed at: University of Pennsylvania School of Medicine, Stellar-Chance Building Room 313, 422 Curie Boulevard, Philadelphia, PA 19104, USA. Tel: +1 2158980305; Fax: +1 2155736728; Email: stamboli@mail.med.upenn.edu

been detected in adult brain as well as embryonic tissues (kidney, brain, eye and tooth primordial) (9,10), the function and expression of the NHS1 protein have not been examined. In this report, we examine the mouse *Nhs1* gene, which is located in the *Xcat* critical region. We determine that *Xcat* mice do not have *Nhs1* coding region mutations but do carry a large insertion mutation within the first intron of *Nhs1*. We show that both expression of the *Nhs1* transcript and the *Nhs1* gene product are altered in *Xcat* mice. Finally, we show that exon 1 is the critical element of the gene to target the protein to the cytoplasm. Without exon 1, the Nhs1 protein is localized to the nucleus.

RESULTS

The mouse *Xcat* mutation was originally mapped by our laboratory within the 2.11 Mb *Xcat* critical region from DXMit20 to DXMit121 (Fig. 1A). Our previous work examined several genes within this region and did not detect any mutations in the exons or intron boundaries of these genes (7,8). To aid in our search of the entire *Xcat* critical region for mutations, we generated BAC libraries from our mutant *Xcat* mouse. A contig consisting of 16 BAC clones made a minimal tiling path spanning 2.11 Mb and provided close to 90% coverage of the region (Fig. 1A).

As expected, most of the 32 BAC-end sequences mapped to the *Xcat* critical region. However, the screen identified two adjacent BACs (BAC8 and BACN01; Fig. 1) that each contained a BAC-end mapping to an entirely different region of the X-chromosome. The non-sequitur sequences within BAC8 and BACN01 were both from a more proximal region of the X-chromosome located 102 Mb from the centromere, whereas *Xcat* is located 155 Mb from the centromere (NCBI build 34). These results are consistent with the presence of a large insertion mutation within the *Xcat* critical region. To explore this further, we performed additional sequence analysis directly on BAC8 and BACN01 and determined where the non-sequitur ends are joined with the *Xcat* critical region DNA. Primers were designed to amplify these junction sites, and PCR was performed on genomic DNA from normal and *Xcat* animals. As expected, no junction-site PCR product was produced using genomic DNA from normal mice. However, the translocation junction sites were successfully amplified from *Xcat* genomic DNA, indicating that the X-chromosome rearrangement is present in *Xcat* genomic DNA and is not an artifact of BAC library construction (data not shown). PCR was also performed using primers surrounding the normal position of the translocated fragment to determine whether the inserted fragment was also in its normal chromosome location in *Xcat* mice. Product was produced in normal and *Xcat* samples, indicating that the translocated fragment was duplicated and translocated into the *Xcat* critical region (data not shown). Sequence analysis of the two junction fragments revealed that no *Xcat* critical region sequence was lost during the insertion event and that the size of the inserted fragment is 487 kb.

BAC FISH

To confirm the presence of this insertion, we analyzed *Xcat* chromosomes by FISH, probing with three fluorescently

labeled overlapping BACs from the 487 kb duplicated fragment (RP23-166N12, RP23-284F8, RP23-18K13; Fig. 1C). Each labeled BAC was tested independently and all three gave identical results. As expected, the BACs labeled one distinct region on WT mouse X-chromosome (Fig. 2B). In contrast, chromosomes from *Xcat* mice were labeled in two distinct spots (Fig. 2D), one corresponding to the normal position of this sequence (102 Mb region) and another at the telomere corresponding to the *Xcat* critical region (155 Mb region). This further confirmed our impression that a duplication and translocation event occurred on the X-chromosome in the *Xcat* mutant.

Transcription of *Nhs1*

The mouse *Nhs1* gene was modeled by aligning human mRNA AY436752 against mouse genomic DNA. The structure of the mouse cDNA was then confirmed by amplifying and sequencing RT-PCR products. No coding region mutations were identified in *Nhs1* cDNA from *Xcat* when compared with wild-type (WT) for exons 2 through 8. However, spliced *Nhs1* products containing exon 1 were readily amplified from WT cDNA but not from *Xcat*, suggesting that the 5' end of *Nhs1* is spliced differently in *Xcat*. Analysis of WT E14.5 whole embryo cDNA by 5'-RACE identified an alternate transcription start site (exon 1A) that produces a new variant of *Nhs1_v1* (Fig. 1B). A human cDNA clone (CR936788) was recently isolated from retina and is the human homolog of *Nhs1_v1*. Thus, both mice and humans produce a variant of this gene. It is important to note that mouse exon 1A is different from human exon 1B and likewise mouse *Nhs_v1* is distinct from human Nhs isoform B (10).

In WT mice, *Nhs1* exon 1 is separated from exon 2 by a large 283 kb intron. In *Xcat*, the 487 kb insertion maps within this first intron, resulting in a separation of exon 1 from exon 2 by 770 kb (Fig. 1C). To determine whether the insertion affects the transcription of *Nhs1*, we monitored *Nhs1* transcription by performing RT-PCR on selected embryonic tissues. NHS patients have eye, tooth and digit abnormalities, indicating that *NHS1* is required for the proper formation of these tissues. As such, *NHS1* message should be expressed in these tissues during development. For this reason, we examined the expression of *Nhs1* in the developing eye, mouth and paw of normal and *Xcat* mice. Tissues were dissected from embryos (E14.5) and RNA was extracted and analyzed by RT-PCR, using *Nhs1* primers designed to amplify transcripts containing either exons 1 through 3 or exons 1A through 3. The transcript beginning with exon 1A was present in all tissues assayed in both normal and *Xcat* mice. In contrast, the transcript beginning with exon 1 was readily found in normal mice but was not detectable in *Xcat* cDNA (Fig. 3A).

To quantify the difference in expression of *Nhs1* and its variant *Nhs_v1*, relative amounts of the two *Nhs1* forms were measured in E14.5 eyes by quantitative real time RT-PCR. As shown in Table 1, comparable amounts of *Nhs1_v1* transcript were detected in WT and *Xcat* samples. In contrast, *Nhs1* transcript was essentially absent in *Xcat* samples, yet was readily amplified in WT samples, confirming the previous

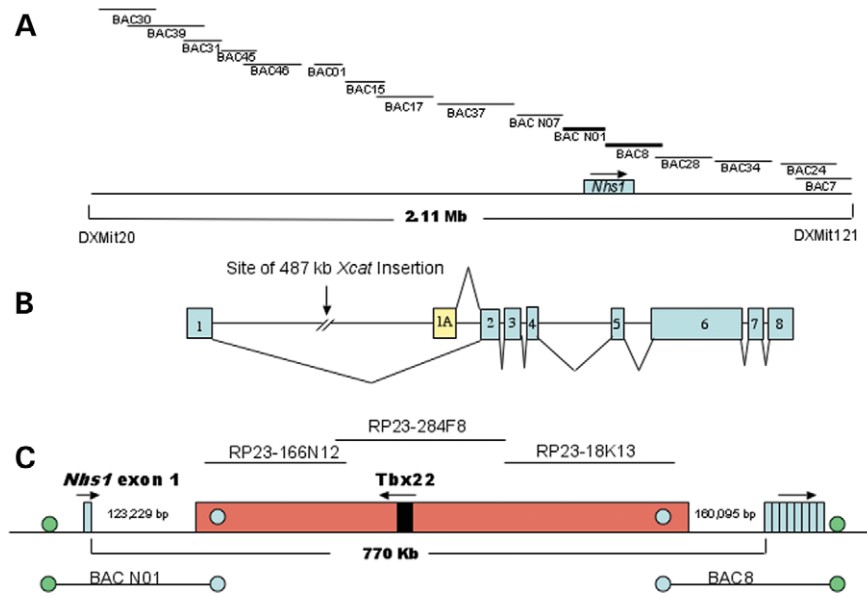


Figure 1. Gene structure of *Nhs1* in normal and *Xcat*. (A) Schematic map of the *Xcat* critical region between DXMit121 and DXMit120 as well as the position of *Nhs1*. BAC contig constituting the minimal tiling path is displayed within the critical region. The position of *Nhs1* lies within both BAC N01 and BAC 8. All BAC clones were derived from *Xcat* genomic DNA and end-sequenced to position them within the *Xcat* critical region. (B) Mouse *Nhs1* gene structure showing relative positions of exons 1 and 1A and location of the 487 kb insert within intron 1. (C) Location of the 487 kb insert within intron 1 with respect to overlapping BACs. The BAC ends from BAC 8 and BAC N01 contain sequence from the translocated insert as well as the normal sequence from the critical region. Three BACs, RP23-166N12, RP23-284F8 and RP23-18K13, map to the 487 kb insert and were used as probes in the FISH experiments. Note that the *Tbx22* gene is located within the 487 kb insert.

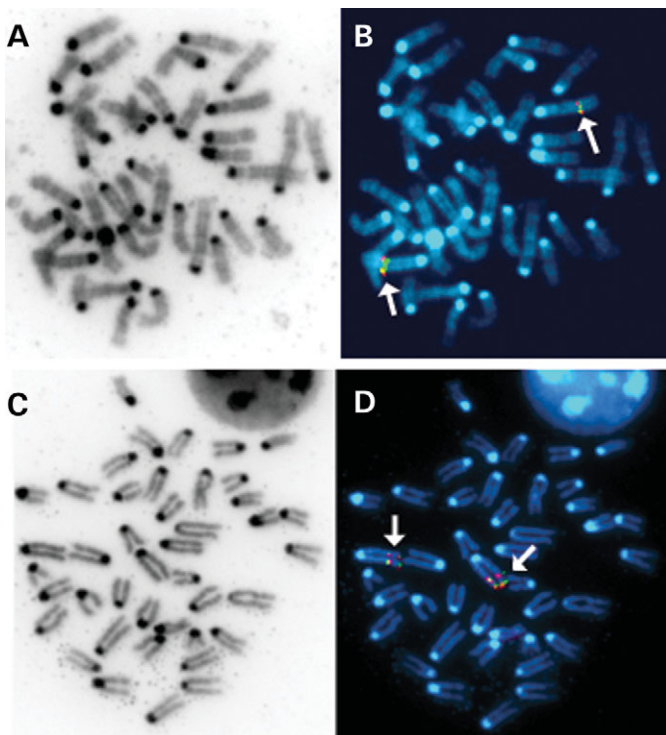


Figure 2. BAC FISH analysis of female X-chromosomes showing duplication in *Xcat*. BAC clones RP23-284F8, RP23-166N12 and RP23-18K13, which map to the 487 kb insert were labeled and used to probe normal (A and B) and *Xcat* (C and D) chromosomes. The hybridized regions appear red (arrow). Identical results were obtained using all three clones and results from RP23-166N12 are shown. Note the double signal signifying the duplication in *Xcat* when compared with that in normal.

RT-PCR analysis. These results indicate that the large insertion within *Nhs1* intron 1 results in a deficiency of *Nhs1* in *Xcat* mutants.

The insert contains one known gene (*Tbx22*) which is transcribed in the opposite direction of *Nhs1* (Fig. 1). To examine whether the extra copy of *Tbx22* changes transcription levels of this gene, we measured the levels of *Tbx22* transcript in E14.5 embryos in normal and *Xcat* mice by quantitative RT-PCR and determined that the levels of *Tbx22* transcript in normal and *Xcat* tissues are identical (Table 1).

Nhs1 protein expression in WT and *Xcat* eyes

To determine the effect the insert has on *Nhs1* gene product, antibodies were made against the predicted *Nhs1* protein and used to examine protein expression in normal and *Xcat* mice. The antibody was raised against a C-terminal portion of the protein and should therefore recognize both isoforms 1 and 1A. To test the specificity of the antibody, western blotting was performed on protein extracts from P0 WT tissues. As shown in Figure 3B, our antibody detected a major immunoreactive species in both the kidney and liver samples. Attempts to examine neonate lens extracts by western blotting using our antibody were unsuccessful (data not shown).

In both WT and *Xcat*, the developing lens fills with elongating lens fiber cells (12). To analyze the expression of *Nhs1* protein in lens fibers, immunohistochemical analysis of P0-1 eye tissue was performed. In WT, *Nhs1* staining is predominantly in the developing fiber cells (Fig. 4B). In contrast,

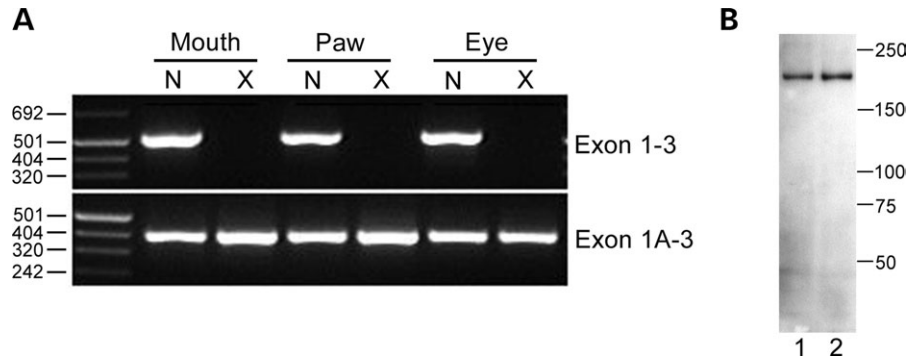


Figure 3. (A) Different expression of *Nhs1* isoforms in normal and *Xcat* tissue. RT-PCR products generated from E14.5 mouth, paw and whole eye cDNA using primers specific for exons 1, 1A and 3 were analyzed by agarose gel electrophoresis. Product representing exons 1–3 was amplified in normal but not in *Xcat* cDNA, whereas exons 1A–3 product was amplified in both normal and *Xcat*. (B) Western blot analysis for *Nhs1* performed on total extracted proteins from P0 WT kidney and liver. Lane 1 is kidney and lane 2 is liver.

Table 1. Quantitative real-time PCR expressed as cycle threshold (C_T) values

	Normal eye C_T	<i>Xcat</i> eye C_T
<i>Nhs1</i>	25.4	>40
<i>Nhs1_v1</i>	27.9	27.1
GAPDH	20.7	21.3
α -Actin	23.3	23.8
<i>Tbx22</i>	27.8	27.7

Nhs1 begins with exon 1 and *Nhs1_v1* begins with exon 1A. GAPDH and actin are controls and *Tbx22* is a gene within the duplicated fragment. C_T is the fractional cycle number at which the fluorescence passes the fixed threshold.

Nhs1 staining in *Xcat* is dramatically reduced (Fig. 4E) and the slight staining observed is clearly distinct from the normal WT staining pattern. One hypothesis for the decreased staining in *Xcat* is a global depression of protein synthesis. In order to investigate this hypothesis, the same section utilized for Figure 4G was stained with aquaporin O (a lens-specific membrane protein) and demonstrated robust staining, suggesting that an overall depression of protein synthesis was not responsible for decreased expression of *Nhs1*.

PSI-BLAST

The mouse *Nhs1* sequence was subjected to position-specific iterated Blast (PSI-BLAST) analysis to identify related proteins (Table 2). The predicted N-terminus of *Nhs1* (encoded by exon 1) is proline-rich and is structurally similar to dynamin and synaptojanin (Region I). These results are intriguing because each of these proteins is known to interact with the actin cytoskeleton and this interaction is mediated at least in part by the proline-rich domain (13,14).

A second region identified by PSI-BLAST is located just downstream and is encoded by a sequence within exons 1–4. This region is significantly similar to the WH1 domain of the WASP (Wiscott–Aldrich syndrome protein) and

WAVE proteins (Table 2, Region II). WASP was first identified as the protein defective in patients with Wiskott–Aldrich syndrome (WAS). The majority of point mutations found in WAS-affected patients occur within the N-terminus of WASP, a region designated WH1 (Wiskott–Aldrich homology). It has been shown that the WH1 domain is necessary and sufficient for the interaction of WASP to associate with Abi1, and Arp2/3, proteins that function in actin remodeling (15,16).

A third region (Region III, Table 2) of *Nhs1*, encoded by an exon 6 sequence, was found to be structurally related to the bestrophin protein, an anion transporter expressed on the basal lateral surface of RPE cells and the gene defective in macular dystrophy BEST disease (17). The region of similarity maps to the C-terminus of the bestrophin protein, an area of unknown function (Table 2).

The encoded amino acids of exon 1A was used as a seed query for the first iteration of PSI-BLAST to search the non-redundant database. There were no significant matches to this query input.

Nhs1–GFP fusion protein analysis

Our RNA expression analysis indicates that *Xcat* mice express *Nhs1* isoform 1A but not isoform 1 (Fig. 3A). To explore the biological difference between these isoforms, we performed expression analysis of *Nhs1*–GFP fusion proteins in transfected CHO cells. Expression vectors were constructed containing GFP fused at its N-terminus with either *Nhs1* exons 1 through 5 (*Nhs1*–GFP) or *Nhs1* exons 1A through 5 (*Nhs1A*–GFP). CHO cells transfected with these constructs were then examined by fluorescence confocal microscopy. As shown in Figure 5 (C and D), *Nhs1*–GFP fusion proteins are present in a punctate distribution within the cytoplasm. In contrast, *Nhs1A*–GFP fusion proteins had a definitive nuclear localization as evidenced by their colocalization with nuclear DAPI staining (Fig. 5A and B). These studies indicate that *Nhs1* is a localized cytoplasmic protein and *Nhs1_v1* is targeted to the nucleus.

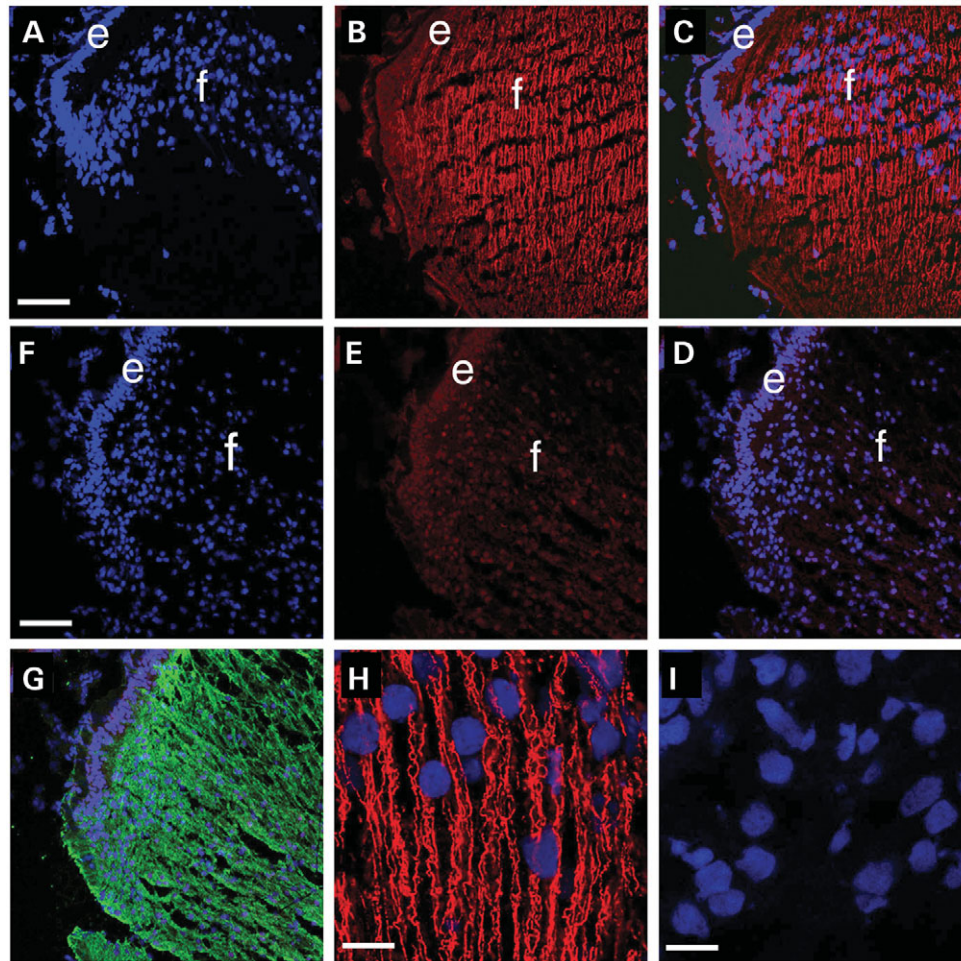


Figure 4. Immunohistochemistry of newborn lenses from WT and *Xcat* mice. Transverse sections from WT (A–C) and *Xcat* mouse lenses (D–F) were stained for Nhs1 (red) and counterstained with ToPro3 which detects cell nuclei (blue). Merged images are shown in (C) and (F). Nhs1 staining is found at moderate levels in the lens epithelium (e) and higher levels are found in lens fiber cells (f) in a filamentous distribution running parallel to their long axis in WT mice (B, C and H). However, this staining pattern is absent from lenses of *Xcat* mice (E, F and I). Staining of *Xcat* lens with aquaporin O (G, green) demonstrates intense staining, suggesting that protein synthesis is not generally depressed. High power view of Nhs staining in WT lens fibers (H) and its absence in the fibers of the *Xcat* lens (I). (A–G) are 200 \times magnification (bar = 77 μ m) and (H) and (I) are approximately 1200 \times magnification (bar = 13 μ m).

Table 2. PSI-BLAST analysis of Nhs1 protein sequence identifying functional regions of the Nhs1 protein

Region	Amino-acids	Gene	Function of homologous region	Reference
I	1–107	Dynamin	Binds actin	(14)
	1–107	Synaptojanin	Binds actin	(13)
II	112–249	WAVE	Abil binding	(16)
	112–249	WASP	Binds actin/actin BP	(16)
III	883–1068	Bestrophin	Ion channel transport	(17)

DISCUSSION

This study describes the genetic defect in *Xcat* mice, the first animal model for human NHS. By examining a BAC library made from *Xcat* genomic DNA, we were able to identify a large 487 kb insert within the first intron of the mouse *Nhs1* gene. The 487 kb insert originated from a position on the

X-chromosome 45 kb away from the *Xcat* critical region. Quantitative real-time PCR verified that the insertion in intron 1 results in suppression of expression of mRNAs containing exon 1. Transfection studies of CHO cells confirm the importance of the exon 1-encoded amino acid sequence to target the protein to the cytoplasm. The alternative variant *Nhs_v1* (lacking exon 1) is targeted to the nucleus. Antibodies made against Nhs1 strongly stain the lens fiber cells of newborn WT mice. In contrast, *Xcat* lenses display very low levels of Nhs1 staining and this limited staining appears nuclear.

There are a number of reasons that might explain why exon 1 is not present in *Xcat Nhs1* transcripts. The large inserted fragment changes the structure of *Xcat* intron 1 and could interrupt efficient splicing of exon 1 to exon 2. Perhaps, intron 1 contains specific sequences required for efficient splicing of exon 1 to exon 2 and this sequence is disrupted by the insert. Alternatively, exon 1 may be spliced to a different novel exon in the presence of the extra insert sequence,

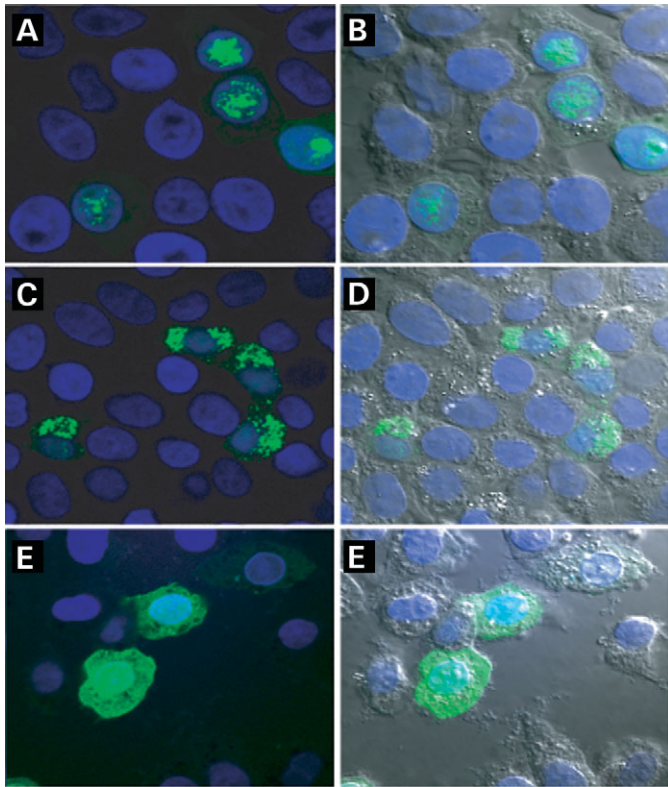


Figure 5. Confocal fluorescence microscopy of transfected CHO cells showing subcellular localization of Nhs1–GFP and fusion proteins. *Nhs1* exons 1 through 5 or 1A through 5 were cloned in frame to the 5' end (N-terminus) of GFP. The resultant vectors were transfected into CHO cells and the localization of the Nhs1–GFP fusion proteins was examined. CHO cells expressing protein from exons 1 to 5 constructs display a cytoplasmic expression pattern, whereas cells expressing protein from exons 1A to 5 display nuclear expression. (A and B) are the fluorescence and DIC micrograph of fusion proteins constructed from exons 1A to 5. (C and D) are the representative micrographs of fusion proteins constructed from exons 1 to 5 and (E and F) represent the GFP vector without insert (green, GFP, blue, DAPI nuclear staining).

making it unavailable for incorporation into *Nhs1* transcripts. It is also possible that exon 1 splices to cryptic exons from the insertion, which in turn splice to exon 2. This could produce a transcript with a long insertion between exons 1 and 2, which is too long to detect in the RT–PCR reaction. In turn, this could produce a larger or frame-shifted version of the Nhs1 protein with bad consequences for the cell. Regardless of the mechanism, the relationship between the presence of the insert and the deficiency of isoform 1 transcripts is strong and provides evidence that alteration of the *Nhs1* gene causes the *Xcat* phenotype.

The RNA expression studies indicate that E14.5 mice express at least two *Nhs1* isoforms, whereas *Xcat* mice only express the *Nhs1_v1* isoform. The antibody used in our study does not discriminate between the two isoforms. Therefore, unless the two isoforms have different molecular weights that can be separated on acrylamide gels, we would not expect to detect both isoforms. In order to better explore the presence of the different isoforms that occur between tissues and during development, we are currently making isoform-specific

antibodies. Such antibodies can then be used as probes to detect the different forms of Nhs1 that occur during development and between tissues. Comparative isoform analysis between WT and *Xcat* should provide further insight into the pathophysiological mechanism of *Xcat*.

Our PSI-BLAST analysis identified two domains at the N-terminus of the Nhs1 protein, which are known to target proteins to the cytoskeleton. The first, a poly-proline domain, is homologous to the poly-proline domain in both dynamin and synaptojanin. Alteration of this region in either of these two proteins results in protein that no longer associates with the cytoskeleton (13,14). The poly-proline domain of Nhs1 is encoded entirely from a sequence within exon 1. Likewise, the second domain identified on Nhs1 is a WH1 domain which is required by both WASP family proteins to associate with actin and regulate actin dynamics through interaction with Arp2/3 (16). Half of this domain is encoded by a sequence found in exon 1. If association with the cytoskeleton is required for Nhs1 function, then the lack of the exon 1-encoded sequence could prevent association with the cytoskeleton and result in non-functional protein.

Our data also suggest that the N-termini of both *Nhs1* isoforms have targeting information for these proteins. The *in vitro* transfection studies suggest that the N-terminus of *Nhs1_v1* directs the protein to the nucleus. There are four predicted nuclear localization signals in both the human NHS1 and mouse Nhs1 proteins (10); none has been examined functionally. It is possible that in the absence of the exon 1-encoded sequence, the nuclear localization signals in *Nhs1_v1* are more efficiently recognized by the nuclear import machinery. The presence of the exon 1-encoded sequence in Nhs1 might mask the nuclear localization signals, forcing localization of the protein to the cytoplasm.

It is noteworthy that two studies of NHS patients have identified probands with no *NHS1* coding region mutations (9,10). It would be interesting to see whether these individuals carry regulatory mutations that are similar to our *Xcat* mutant. It would be difficult to examine this at the genomic DNA level but if *NHS1*-expressing tissue could be obtained from these patients, the relative amounts of *NHS1* isoforms could be measured. Another intriguing finding from human NHS patients is the identification of NHS families with exon 1 truncation mutations (9–11). This is very analogous to our mutant and further highlights the importance of exon 1 for functional NHS1 protein.

The X-ray induced mutation present in *Xcat* animals appears to be the result of segmental duplication coupled with an intrachromosomal rearrangement. Our data indicate that these events disrupted the *Nhs1* gene in *Xcat*, resulting in cataracts. Although the inserted fragment contains the *Tbx22* gene, we found no evidence that the expression of *Tbx22* was altered in *Xcat*.

This study reports the identification of an insertion mutation within the mouse *Nhs1* gene, which leads to altered expression of *Nhs1*. On the basis of the molecular characterization of the mutation, we designate the mutant allele symbol *Nhs1^{Xcat}*. It will be important to examine the function of this protein and explore its role in development. With regard to lens development, the protein does not share structural homology to other genes with known roles in this process, such as crystallins,

aquaporin and connexins. Moreover, the protein has at least two isoforms, and the importance of these isoforms in different tissues will need to be determined. In addition, *Nhs1* tissue-specific expression, developmental tissue expression and subcellular localization as well as the identification of *Nhs1*-interacting proteins will be important steps toward determining how this protein functions.

MATERIALS AND METHODS

Mice

The original *Xcat* mutation was recovered in an F1 female descendant of the cross T-stock female X DBA/2 irradiated male in which the offspring were screened for dominant cataract (3). The animals in this study are inbred descendants of a mating between a DBA/2 female homozygous for the *Xcat* mutation and C57BL/6.

BAC library construction and analysis

Genomic DNA was isolated from *Xcat* mouse liver using standard techniques and embedded into HMW DNA agarose plugs to maintain DNA integrity. Plugs containing DNA were partially digested with either *Bam*H1 or *Hind*III under conditions that favor the generation of large 100–150 kb fragments which were then ligated into the appropriate site of the BAC vector pECBAC1. About 93 000 recombinant clones were robotically picked and arrayed in duplicate onto 384-well plates and then spotted onto nylon filters.

Filters containing the mutant *Xcat* library were screened with overgo probes designed against sequences across the entire *Xcat* critical region (Fig. 1A). Primers to make overgo probes were designed using the Overgo Maker Tool (<http://www.genome.wustl.edu/tools/overgo>). Overgo labeling was carried out as described (18). Briefly, for each overgo probe, two overlapping oligonucleotides were combined and incubated at 80°C for 5 min, followed by 10 min at 37°C. Labeling of the overgo probes was accomplished by adding overgo labeling buffer (18), 5 μ Ci each of [α -³²P]dATP and [α -³²P]dCTP, 2 U Klenow enzyme and incubating at 37°C for 1 h. Unincorporated nucleotides were removed using Sephadex G50 spin columns, and labeled probes were incubated at 90°C for 10 min before hybridization to the filter. Filters were pre-hybridized at 60°C in Church's hybridization buffer for 1 h and hybridized overnight with overgo probes at 60°C. They were then washed two times each with 2 \times SSC/0.1% SDS, 1.5 \times SSC/0.1% SDS and 0.75 \times SSC/0.1% SDS and exposed to film. BAC DNA from positive clones was isolated using Qiagen Q500 columns and a modified protocol with larger lysis, neutralization and wash volumes as recommended by the manufacturer. BAC-end sequences were obtained by sequencing the purified BACs directly with T7 or SP6 primers using ABI dye-terminator chemistry (ABI, Woodlands, CA, USA) and an ABI 3900 sequencer. BACs were assembled into a contig by mapping BAC-end sequences onto the *Xcat* critical region reference sequence found on the UCSC genome browser (<http://genome.cse.ucsc.edu/>). Entire BACs were sequenced by both primer walking and shot gun sequencing.

BAC FISH

Fluorescent *in situ* hybridization was performed essentially as described (19,20). DNA from the BAC clones RP23-284F8, RP23-166N12 and RP23-18K13, representing the duplicated DNA, were labeled with Spectrum Orange (Vysis, Downers Grove, IL, USA) by nick translation. Chromosome slides were incubated with 200 ng labeled probe and 2 mg of Cot1 DNA. Slides were counterstained with DAPI-Antifade (250 ng/ μ l; BM Vector, Burlingame, CA, USA).

PCR and RT-PCR

Genomic DNA was isolated from mouse liver and used as template in PCR experiments as described (8). Total RNA was prepared from wild-type or mutant *E14* embryos using the RNAqueous-4 PCR kit and reverse transcribed using the RETROscript kit, all according to the manufacturer's suggested protocols (Ambion, Austin, TX, USA). For RT-PCR, reverse transcription reactions (1–5 μ l) were amplified using cDNA-specific primers and for PCR, genomic DNA (100 ng) was amplified using primers that span intron–exon junctions. PCR on both templates was performed with 0.5 U AmpliTaq gold polymerase (ABI, Forrest City, CA, USA), 10 mM Tris–HCl pH 8.3, 1.5 mM MgCl₂ and 50 μ M each of dATP, dTTP, dGTP and dCTP in 50 μ l volume. Amplification was carried out using the following conditions: 94°C for 5 min, followed by 35 cycles of 95°C for 1 min, 55°C for 30 s, and 72°C for 1 min and a final extension at 72°C for 7 min. PCR products were separated by gel electrophoresis, purified over gel filtration columns (Novagen, Madison, WI, USA) and cloned into TOPO II vectors (Invitrogen, Carlsbad, CA, USA) or sequenced directly on a 3900 DNA Sequencer (Applied Biosystems, Forrest City, CA, USA).

Quantitative, real-time PCR was carried out on an ABI Prism 7900HT sequence detection system using TaqMan chemistry with GAPDH and α -actin as controls (all reagents, detectors and software from PE Applied Biosystems). Amplification of specific PCR products was detected using dual-fluorescent non-extendable probes labeled with 6-carboxy-fluorescein (FAM) at the 5' end and 6-carboxytetramethylrhodamine (TAMRA) at the 3' end. Amplification of each target gene from each RNA probe was carried out in triplicate in separate 25 μ l reactions within 384-well MicroAmp optical plates. Reactions contained 1 \times TaqMan Buffer, 4 mM MgCl₂, 20 μ M of each dNTP, 300 μ M forward and reverse primers, 40 nM dual-labeled fluorogenic probe, 1.25 U AmpliTaq Gold DNA polymerase and 5–50 ng cDNA. Reaction conditions were 95°C for 10 min followed by 40 cycles of 95°C for 15 s and 60°C for 1 min.

Targets were amplified from serially diluted E14.5 eye cDNA to verify optimal amplification efficiencies for each set of primers. Amplification of each specific gene was calculated as a relative amount to two control genes—GAPDH and α -actin. Control samples that were not reverse transcribed showed no significant signal with all primers, indicating that the signal is not due to contaminating genomic DNA within the RNA preps. Data analysis utilized the Sequence Detector Software System to determine baseline and threshold cycle (C_T) values for amplified products.

PSI-BLAST analysis

To ascertain regions of potential functional conservation, PSI-BLAST similarity searches were performed using *Nhs1* against various databases (all vertebrates). To increase search specificity, conserved subsequences were selected as a seed for new PSI-BLAST searches in the vertebrate and invertebrate databases. Nhs conserved subsequences selected included residues 1–120, 121–300 and 1000–1250. All searches were performed using a minimum of four iterations, low complexity filtering and a word size of 2 ($W = 2$). The inclusion threshold for subsequent iterations was set at the 0.005 significance level. Matrix selection was variable based on evolutionary distance of the database chosen (e.g. BLOSUM45 for fungi database). All regions of conservation identified in *Nhs1* were also searched against the PFAM families database of alignments and Hidden Markov models.

Antibody production

A sequence containing a portion of *Nhs1* exon 6, all of exon 7 and a portion of exon 8 (encoding amino acids 1362–1633) was amplified by PCR from normal P0 eye cDNA. The resultant *Nhs1* fragment was cloned into the MCS of pGEX5 to generate a sequence encoding an *Nhs1*–GST fusion protein. The plasmid was transformed into XL-1 cells which were induced to express the fusion protein by growth in IPTG. The GST-fusion protein was recovered from bacterial cell lysates with glutathione–Sephadex chromatography. The glutathione-bound material was separated by PAGE, gel purified and extensively dialyzed to remove residual SDS. The fusion protein was then used to immunize chickens. Chicken sera were tested by ELISA for immunoreactivity against the *Nhs1*–GST fusion protein. Chicken IgG (IgY) was purified from eggs produced by positive chickens and further affinity-purified using immobilized *Nhs1*–GST antigen following standard procedures.

Western blot analysis was done to show specificity of the antibody. Aliquots of 50 µg total protein from P0 WT kidney and liver were run on 10% acrylamide gel and then transferred onto a PVDF membrane (Hybond-P). Western blotting analysis for *Nhs1* was performed using 1:400 diluted antibody (anti-mouse *Nhs1*). HRP-rabbit anti-chicken Ig (catalog and company) secondary antibody (1:50 000) and the ECL Plus chemiluminescent protein detection kit (Amersham Bioscience) were used.

Immunohistochemistry of *Nhs1*

Immunohistochemical staining for *Nhs1* was performed using the techniques previously described (21). Briefly, lenses were excised from newborn mice and embedded directly in OCT (Tissue Tek). Tissue was sectioned at 16 µm and mounted onto Colorfrost/Plus slides (Fisher Scientific, Pittsburgh, PA, USA). Slides were fixed with ice cold 1:1 acetone:methanol for 10 min and air dried prior to further processing. All slides were blocked with 1% BSA in 1× PBS for 1 h at room temperature. Anti-*Nhs1* IgY was diluted 1:500 in 1% BSA–PBS, layered over the section and incubated for 1 h at room temperature. The slides were washed twice with

1× PBS and then incubated for 1 h at room temperature with a 1:250 dilution of goat-anti chicken Alexa Fluor 568 conjugate (Molecular Probes, Eugene, OR, USA) in 1% BSA/PBS containing a 1:2000 dilution of the nucleic acid stain To-Pro3 (Molecular Probes). The slides were again washed twice with 1× PBS and then mounted. The slides were viewed on a Zeiss 510 LSM confocal microscope with an argon/krypton laser (Zeiss, Gottingen, Germany). Double labeling experiments were performed by adding rabbit polyclonal antibodies against aquaporin O/MIP (1:400 dilution, AB3071 Chemicon International) to the solution containing the anti-*Nhs1* primary antibody. These antibodies were detected by adding AlexaFluor 488 labeled goat anti-rabbit IgG to the secondary antibody staining solution described earlier.

Nhs1–GFP fusion protein production and analysis

Nhs1 regions containing exons 1–5 or exons 1A–5 were amplified from WT E14.5 whole eye cDNA, cloned into pCRII–TOPO vectors (Invitrogen) and sequenced. Fragments were then subcloned into pEGFP–N2 expression vectors (BD Biosciences, Palo Alto, CA, USA). Cultured CHO cells, growing in F-12K with 10% FBS, were transfected with GFP-fusion protein vectors using Fugene 6 reagent (Roche Molecular Biochemicals). Thirty-six hours post-transfection, cells were fixed in 70% ethanol and stained with DAPI. Samples were examined for GFP expression with a Zeiss LSM510 META laser scanning confocal module on a Zeiss Axiovert 200M inverted microscope using the Plan Apo 63×/1.4 oil DIC and Plan Neo 25×/0.85 multi DIC objectives. Image data were analyzed using Zeiss LSM510 META v3.2 software.

ACKNOWLEDGEMENTS

The authors wish to thank Robert Nussbaum, MD, for his insight and guidance throughout this project as well as Shakimma Turner for performing the histology of the mouse lens. This study was supported, in part, by US Public Health National Eye Institute grant RO1 EY13615 (K.M.H.) and RO1 EY15279 (M.K.D.) and the Delaware Institutional Networks for Biomedical Research Excellence Award, P20 RR16472 (University of Delaware).

Conflict of Interest statement. None declared.

REFERENCES

- Horan, M. and Billson, F. (1974) X-linked cataract and hutchinsonian teeth. *Aust. Paediatr. J.*, **10**, 98–102.
- Lewis, R.A., Nussbaum, R.L. and Stambolian, D. (1990) Mapping X-linked ophthalmic diseases. IV. Provisional assignment of the locus for X-linked congenital cataracts and microcornea (the Nance–Horan syndrome) to Xp22.2–p22.3. *Ophthalmology*, **97**, 110–120; discussion 120–121.
- Favor, J., Neuhauser-Klaus, A. and Ehling, U.H. (1987) Radiation induced forward and reverse specific locus mutations and dominant cataracts mutations in treated BALB/c and DBA/2 mice. *Mutat. Res.*, **177**, 161–169.

4. Favor, J. and Pretsch, W. (1990) Genetic localization and phenotypic expression of X-linked cataract (Xcat) in *Mus musculus*. *Genet. Res.*, **56**, 157–162.
5. Grimes, P.A., Favor, J., Koeberlein, B., Silvers, W.K., Fitzgerald, P.G. and Stambolian, D. (1993) Lens development in a dominant X-linked congenital cataract of the mouse. *Exp. Eye Res.*, **57**, 587–594.
6. Stambolian, D., Favor, J., Silvers, W., Avner, P., Chapman, V. and Zhou, E. (1994) Mapping of the X-linked cataract (Xcat) mutation, the gene implicated in the Nance–Horan syndrome, on the mouse X chromosome. *Genomics*, **22**, 377–380.
7. Zhou, E., Favor, J., Silvers, W. and Stambolian, D. (1995) Exclusion of three candidate genes, *Grpr*, *Cx33*, and *Pdha1*, for the X-linked cataract gene on the distal region of the mouse chromosome X. *Mamm. Genome*, **6**, 357–359.
8. Huang, K.M., Geunes-Boyer, S., Wu, S., Dutra, A., Favor, J. and Stambolian, D. (2004) Organization and annotation of the Xcat critical region: elimination of seven positional candidate genes. *Genomics*, **83**, 893–901.
9. Brooks, S.P., Ebenezer, N.D., Poopalasundaram, S., Lehmann, O.J., Moore, A.T. and Hardcastle, A.J. (2004) Identification of the gene for Nance–Horan syndrome (NHS). *J. Med. Genet.*, **41**, 768–771.
10. Burdon, K.P., McKay, J.D., Sale, M.M., Russell-Eggitt, I.M., Mackey, D.A., Wirth, M.G., Elder, J.E., Nicoll, A., Clarke, M.P., Fitzgerald, L.M. *et al.* (2003) Mutations in a novel gene, *NHS*, cause the pleiotropic effects of Nance–Horan syndrome, including severe congenital cataract, dental anomalies, and mental retardation. *Am. J. Hum. Genet.*, **73**, 1120–1130.
11. Ramprasad, V.L., Thool, A., Murugan, S., Nancarrow, D., Vyas, P., Rao, S.K., Vidhya, A., Ravishankar, K. and Kumaramanickavel, G. (2005) Truncating mutation in the *NHS* gene: phenotypic heterogeneity of Nance–Horan syndrome in an Asian Indian family. *Invest. Ophthalmol. Vis. Sci.*, **46**, 17–23.
12. Grimes, P.A., Favor, J., Koeberlein, B., Silvers, W.K., Fitzgerald, P.G. and Stambolian, D. (1993) Lens development in a dominant X-linked congenital cataract of the mouse. *Exp. Eye Res.*, **57**, 587–594.
13. Stefan, C.J., Padilla, S.M., Audhya, A. and Emr, S.D. (2005) The phosphoinositide phosphatase Sjl2 is recruited to cortical actin patches in the control of vesicle formation and fission during endocytosis. *Mol. Cell. Biol.*, **25**, 2910–2923.
14. Lee, E. and De Camilli, P. (2002) Dynamin at actin tails. *Proc. Natl Acad. Sci. USA*, **99**, 161–166.
15. Innocenti, M., Zucconi, A., Disanza, A., Frittoli, E., Areces, L.B., Steffen, A., Stradal, T.E., Di Fiore, P.P., Carlier, M.F. and Scita, G. (2004) Abi1 is essential for the formation and activation of a WAVE2 signalling complex. *Nat. Cell Biol.*, **6**, 319–327.
16. Stradal, T.E., Rottner, K., Disanza, A., Confalonieri, S., Innocenti, M. and Scita, G. (2004) Regulation of actin dynamics by WASP and WAVE family proteins. *Trends Cell Biol.*, **14**, 303–311.
17. Tsunenari, T., Sun, H., Williams, J., Cahill, H., Smallwood, P., Yau, K.W. and Nathans, J. (2003) Structure–function analysis of the bestrophin family of anion channels. *J. Biol. Chem.*, **278**, 41114–41125.
18. Ross, M.T., LaBrie, S., McPherson, J. and Stanton, V.P. (1999) Screening large insert libraries by hybridization. In Boyd, A. (ed.), *Current Protocols in Human Genetics*. Wiley, NY, pp. 5.6.1–5.6.52.
19. Lichter, P., Cremer, T., Borden, J., Manuelidis, L. and Ward, D.C. (1988) Delineation of individual human chromosomes in metaphase and interphase cells by *in situ* suppression hybridization using recombinant DNA libraries. *Hum. Genet.*, **80**, 224–234.
20. Pinkel, D., Gray, J.W., Trask, B., van den Engh, G., Fuscoe, J. and van Dekken, H. (1986) Cytogenetic analysis by *in situ* hybridization with fluorescently labeled nucleic acid probes. *Cold Spring Harb. Symp. Quant. Biol.*, **51**, 151–157.
21. Reed, N.A., Oh, D.J., Czymmek, K.J. and Duncan, M.K. (2001) An immunohistochemical method for the detection of proteins in the vertebrate lens. *J. Immunol. Methods*, **253**, 243–252.